



LAWRENCE
LIVERMORE
NATIONAL
LABORATORY

Climate Feedbacks and their Implications for Poleward Energy Flux Changes in a Warming Climate

M. D. Zelinka, D. L. Hartmann

February 16, 2011

Journal of Climate

Disclaimer

This document was prepared as an account of work sponsored by an agency of the United States government. Neither the United States government nor Lawrence Livermore National Security, LLC, nor any of their employees makes any warranty, expressed or implied, or assumes any legal liability or responsibility for the accuracy, completeness, or usefulness of any information, apparatus, product, or process disclosed, or represents that its use would not infringe privately owned rights. Reference herein to any specific commercial product, process, or service by trade name, trademark, manufacturer, or otherwise does not necessarily constitute or imply its endorsement, recommendation, or favoring by the United States government or Lawrence Livermore National Security, LLC. The views and opinions of authors expressed herein do not necessarily state or reflect those of the United States government or Lawrence Livermore National Security, LLC, and shall not be used for advertising or product endorsement purposes.

**Climate Feedbacks and their Implications for Poleward Energy Flux Changes
in a Warming Climate**

MARK D. ZELINKA * AND DENNIS L. HARTMANN

Department of Atmospheric Sciences, University of Washington, Seattle, Washington

* *Corresponding author address:* Dr. Mark D. Zelinka, Program for Climate Model Diagnosis and Intercomparison
Lawrence Livermore National Laboratory 7000 East Avenue, L-103 Livermore, CA 94551
E-mail: zelinka1@llnl.gov

ABSTRACT

Feedbacks in the climate system determine the efficiency with which the climate system comes back into equilibrium in response to a radiative perturbation. Although feedbacks are integrated quantities, the processes from which they arise have rich spatial structures that alter the distribution of top of atmosphere (TOA) net radiation. Here we investigate the implications of the structure of climate feedbacks for the change in poleward energy transport as the planet warms over the 21st Century in a suite of GCMs in the CMIP3 archive. Using radiative kernels that describe the radiative response at the TOA to small perturbations in temperature, water vapor, and surface albedo, we partition the change in poleward heat flux into the individual feedbacks that cause it.

We find that latitudinal gradients in the strength of cloud and water vapor feedbacks reinforce the pre-existing latitudinal gradient in net radiation at the TOA, requiring that the climate system transport more heat to the poles under transient global warming. By computing the change in surface fluxes over the course of the 21st Century, we further partition the anomalous poleward heat flux between the atmosphere and ocean, and find that reduced heat flux from the high latitude ocean further amplifies the equator-to-pole gradient in atmospheric heat loss. This requires the atmosphere to increase its share of the total poleward heat transport. As is the case for climate sensitivity, the largest uncertainty in the change in poleward transport in these models can be attributed to the SW cloud feedback. Because the radiative cooling of the NH is slightly greater than that of the SH by the end of the century, more heat must be transported northward. This anomalous flux implies that the Intertropical Convergence Zone must shift southward and the midlatitude storm track must shift northward and intensify.

1. Introduction

In the global mean, the amount of energy received at the top of atmosphere (TOA) from the sun is nearly balanced by the amount of longwave energy emitted by the planet. However, this balance does not hold at every location on the planet. Absorbed shortwave (SW) radiation is large in the Tropics and decreases with latitude because of the sphericity of the Earth and the latitudinal gradient of planetary albedo. Because the atmosphere and ocean transport heat poleward, the meridional temperature gradient is less than if every location on the planet were in local radiative equilibrium. Thus, outgoing longwave radiation (OLR) decreases much less dramatically with latitude than absorbed solar radiation. This results in a net surplus of TOA radiation in the Tropics where absorbed SW radiation exceeds OLR and a deficit at high latitudes where OLR exceeds absorbed SW radiation.

The atmosphere and ocean transport energy from the tropical regions of surplus to the extra-tropical regions of deficit. As such, poleward heat fluxes are fundamentally tied to the top of atmosphere radiation budget. Poleward energy transport peaks at about 5 PW at about 30° latitude where oceanic and atmospheric contributions are approximately equal (Vonder Haar and Oort (1973), Trenberth and Solomon (1994), Trenberth and Caron (2001)). Equatorward (poleward) of this latitude, oceanic (atmospheric) transport dominates the poleward energy flux. Heat flux divergence out of the Tropics is equal to the net TOA energy surplus, and heat flux convergence into the extra-tropics is equal to the net TOA energy deficit.

The net radiation balance at the top of the atmosphere must be adjusted to the ability of the internal dynamics of the atmosphere and ocean to transport heat poleward. Held and Soden (2006) have shown that increased poleward heat flux is a robust feature of GCM simulations of global warming. One can argue that the atmospheric meridional heat flux increases because the gradient in moist static energy increases, as Hwang and Frierson (2010) have done, but one must also ask

what diabatic processes maintain that larger gradient in moist static energy. Here we examine those diabatic processes and their change with global mean temperature to better elucidate their critical role in inducing increased poleward energy transport in a warmed Earth. The internal dynamics of the atmosphere and ocean that determine their heat flux and the radiative-convective feedback processes that maintain the meridional heating gradients are essential to the climate response that produces increased energy fluxes in a warmed Earth. Here we emphasize the latter and raise the question of which of these processes has a stronger role in determining the outcome of enhanced poleward energy flux.

Just as net TOA radiation has nonuniform spatial structure in the mean state, so does its anomaly in a warming climate. Because of the strong constraint of energy conservation in the climate system, this structure in anomalous net radiation must be associated with an anomalous poleward heat transport. Wu et al. (2010) have performed an extensive analysis of the change in poleward heat transports in the GFDL CM2.1 model and have related them to the TOA and surface energy budget changes. They demonstrated that a warming climate is associated with anomalous energy gain in the tropical atmosphere relative to the high latitude atmosphere, requiring larger atmospheric poleward transport that is accomplished in part by stronger midlatitude eddies. They show that this enhanced equator-to-pole energy gradient in a warming world is associated with positive water vapor and cloud feedbacks in the Tropics, negative cloud feedback at high latitudes, enhanced heat uptake by the Southern Ocean, and increased emission to space in the northern high latitudes.

This work extends the work of Wu et al. (2010) to assess the changes in TOA and surface radiation and their implications for changes in poleward heat transport in a suite of GCM simulations performed for the IPCC AR4. A unique feature of this study is the use of radiative kernels (Soden et al. (2008)) to partition TOA radiative flux anomalies and their implied poleward heat transport

anomalies into specific feedbacks in the climate system. Such an approach is appealing because it allows us to separate those aspects that are robust and well-constrained from those that are less robust and more poorly constrained across models. Our results in general support those of Wu et al. (2010), and strengthen the claim that water vapor and cloud feedbacks in the climate system act not only to amplify the global mean surface temperature response to CO₂ forcing, but also to increase the poleward heat transport by the climate system as the planet warms. Furthermore, inter-model spread in the magnitude and spatial structure of cloud feedback (primarily SW cloud feedback) results in inter-model spread in the implied poleward heat transport accompanying global warming. Finally, it is clear from our results that feedback processes affect both the magnitude of global warming and its spatial structure, so that localized feedbacks affect the climate everywhere.

2. Data

We make use of global monthly mean profiles of temperature and humidity, surface temperature, surface and TOA radiative fluxes in both clear and all-sky conditions, and surface latent and sensible heat flux from 15 GCMs in the in the Coupled Model Intercomparison Project Phase 3 (CMIP3) of the World Climate Research Program (WCRP) database (c.f., Table 1).

We compute anomalies of these quantities as the difference in the monthly-mean annual cycle of the last 10 years of the 21st Century in the SRES A2 emissions scenario simulations and the monthly-mean annual cycle of a 30-year climatology computed for the end of the corresponding 20th Century (20c3m) simulations. We use the radiative kernels provided by B. J. Soden, and re-grid all the model data from each model’s native grid onto the same grid as that of the radiative kernels (Soden et al. (2008)). A total of twelve models archived enough data to permit the kernel calculation. Nine of these models archive enough surface flux data to permit partitioning the

poleward flux anomalies between atmosphere and ocean (Table 1).

3. Methodology

The total change in radiation at the top of the atmosphere over the course of the century can be expressed as

$$dR = \Delta\overline{T}_s(f_T + f_q + f_\alpha + f_c) + G, \quad (1)$$

where $\Delta\overline{T}_s$ is the change in global mean surface temperature over the century, f_T , f_q , f_α , and f_c are the radiative feedbacks resulting from changes in temperature (T), water vapor (q), surface albedo (α), and clouds (c), respectively, and G is the radiative forcing in the A2 scenario. In equilibrium, dR is zero by definition. The individual radiative feedbacks (with the exception of clouds) are calculated as

$$f_i = \frac{\partial R}{\partial i} \frac{di}{d\overline{T}_s} \equiv K_i \frac{di}{d\overline{T}_s}. \quad (2)$$

K_i represents the radiative kernel, which expresses the change in TOA radiative flux due to small perturbations in variable i (Soden et al. (2008)). Radiative kernels represent the LW or SW radiative response at the top of atmosphere to temperature, humidity, or surface albedo perturbations at each latitude, longitude, pressure (if applicable), and time. Each kernel is a four-dimensional matrix (latitude, longitude, pressure, and month) that is convolved with the actual model-produced change in variable i and integrated in the vertical to calculate the total TOA flux response. Integration is performed from the surface up to a level that linearly decreases with latitude from 100 hPa at the equator to 300 hPa at the poles, in accordance with Soden et al. (2008). The feedback is computed by dividing the TOA flux response by the change in global mean surface temperature. (For surface albedo feedback there is no pressure dependence and vertical integration is not necessary.) Note

that the feedbacks computed here are defined more loosely than the formal definition (e.g., Hansen et al. (1984)) because we use differences between two transient climate states rather than between two equilibrium states. Also, unlike the formulation of Roe and Baker (2007) and Roe (2009) in which feedbacks are computed relative to a reference system with vertically uniform warming that is considered the basic response of the planet (i.e., the Planck response), we include the TOA flux anomalies due to the temperature response as a feedback. Thus our global feedback values sum to a negative number, indicating that the planet is stable with respect to radiative perturbations.

The radiative kernels are appealing because they allow for relatively simple diagnosis of feedbacks in models using standard monthly mean model output. Additionally, because the term $\frac{\partial R}{\partial i}$ is computed using one model’s radiation code (that of the GFDL atmospheric model version AM2p12b) and then applied across a suite of models, it allows for a consistent computation of the feedbacks across models. This is important because one can unambiguously attribute the spread in feedback estimates to the spread in models’ response patterns rather than to a combination of the response patterns and the radiation code used to compute the feedback in each model.

Cloud feedbacks cannot be computed directly using radiative kernels because the linearity assumption that is required for the kernel to accurately explain TOA fluxes due to small perturbations in individual layers does not apply for cloud field perturbations. One can, however, compute cloud feedbacks by adjusting the change in cloud radiative forcing (defined as the difference between clear-sky and all-sky LW, SW, or net radiative flux at TOA) by the amount of cloud masking in the other feedbacks, as explained in Soden et al. (2008). For each model we calculate the clear and all-sky temperature, water vapor, and surface albedo feedbacks by convolving the appropriate radiative kernels with the change in corresponding variable over the 21st Century. LW cloud feedback is estimated by adjusting the change in LW cloud forcing ($\Delta LWCF$) by the magnitude of cloud masking in the temperature and LW water vapor feedbacks. SW cloud feedback is estimated

by adjusting the change in SW cloud forcing ($\Delta SWCF$) by the magnitude of cloud masking in the SW water vapor and surface albedo feedbacks. The cloud masking is calculated by differencing the clear- and all-sky feedbacks and adding a term due to the cloud masking of the radiative forcing (G) in the A2 scenario (Eqn. 25 of Soden et al. (2008)). We assume that clouds mask the radiative forcing in the SRES A2 scenario by 16%, which is the amount that the GFDL model's radiative forcing due to a doubling of CO_2 is masked by clouds (Soden et al. (2008)). For the last decade of the 21st Century, the global mean LW and SW radiative forcings in the A2 scenario are 6.16 and -0.11 W m^{-2} , respectively (calculated by summing the A2 radiative forcing terms given in Tables 6.14 and 6.15 of the IPCC Third Assessment Report (Ramaswamy et al. (2001))). Thus the 16% cloud masking of the radiative forcing requires the addition of 0.99 W m^{-2} to $\Delta LWCF$ and the subtraction of 0.02 W m^{-2} from $\Delta SWCF$ to calculate the respective cloud feedbacks.

4. Spatial Structure of Climate Feedbacks

The ensemble-mean temperature, water vapor, surface albedo, and cloud feedbacks, along with the combined temperature-water vapor feedback and the sum of all feedbacks are shown in Figure 1. The spatial patterns and global mean values of the feedbacks are comparable with those for the A1B scenario given in Figure 10 of Soden et al. (2008), though the cloud feedback computed here is smaller by $0.11 \text{ W m}^{-2} \text{ K}^{-1}$. The temperature feedback is negative everywhere, indicating that warming the planet causes it to emit more radiation. The feedback is most negative in the Tropics where the upper troposphere warms substantially, over the continents where surface warming is large, and in the Arctic where heating is confined near the surface by large lower tropospheric stability and sea ice loss (Hansen et al. (1984)). The feedback is less negative over the Southern Ocean, where the warming is delayed relative to the rest of the planet.

The water vapor feedback is positive everywhere, with nearly constant relative humidity implying an exponential increase in the absolute abundance of water vapor as the atmosphere warms. This feedback is especially strong in the Tropics due to large fractional increases in humidity that accompany warming in the climatologically dry upper troposphere. As discussed in Soden and Held (2006), large fractional increases in absolute humidity in the tropical upper troposphere are caused by a combination of the large sensitivity of saturation vapor pressure to temperature at very cold temperatures and low pressures (e.g., 15 % K^{-1} at 200 K) as well as the fact that the upper troposphere warms considerably more than the surface due to the maintenance of the moist adiabatic tropical temperature profile as the planet warms.

Cloud feedback is positive (negative) at nearly every location equatorward (poleward) of 45° . This feedback is broken down into its LW and SW components in Figure 2. The LW cloud feedback is positive nearly everywhere, but is especially large where high cloud fraction increases. Zelinka and Hartmann (2010) have shown that the upward shift of high clouds in the Tropics contributes significantly to the positive LW cloud feedback, since high clouds maintain an almost constant temperature as the surface warms. SW cloud feedback is positive throughout the subtropics and negative along the equator and at high latitudes.

The surface albedo feedback is positive and confined to high latitudes, as expected intuitively. The larger fractional coverage of land and therefore greater snow albedo feedback in the Northern Hemisphere (NH) results in a positive surface albedo feedback that extends to lower latitudes than in the Southern Hemisphere (SH).

The sum of all feedbacks when integrated over the entire planet is $-1 \text{ W m}^{-2} \text{ K}^{-1}$, indicating a climate that is stable to perturbations, though significantly less stable than a blackbody planet with no atmospheric feedbacks other than the basic Planck feedback of about $-3.2 \text{ W m}^{-2} \text{ K}^{-1}$ (Hansen et al. (1984); Colman (2003); Soden and Held (2006)). Quite remarkably, the net feedback

map exhibits positive values along the equator in the Pacific. This locally positive net feedback is due to the combination of a relatively strong positive water vapor feedback and strong positive cloud feedback. The latitudinal structure of the feedbacks will be discussed in much greater detail below.

Before continuing it is first necessary to discuss the accuracy of the kernel technique in diagnosing feedbacks. One major source of error in the calculation is the incomplete knowledge of the forcing term (G) in Equation 1. While global mean radiative forcing due to long lived greenhouse gases and sulphate aerosol concentrations is prescribed in the A2 scenario, the total radiative forcing in each model as well as its spatial and temporal structure vary from model to model because modeling centers made use of different socio-economic models (IAMs) that produce emissions projections, made varying assumptions about emissions not provided by the IAMs, and included to varying degrees physical processes like aerosol indirect effects in their simulations (Shindell et al. (2008)). Because neither total radiative forcing nor its spatial structure are archived for the models, our use of a G that is invariant in space and across models introduces error to the calculation of cloud feedback.

Thus, sources of error in our feedback calculation include contributions from model-specific radiative forcings (e.g., due to changes in aerosol loading) that differ from the standard A2 scenario, spatial deviations of the A2 forcing from the global mean forcing reported in Tables 6.14 and 6.15 of the IPCC Third Assessment Report (Ramaswamy et al. (2001)), and errors in the kernel calculation of TOA flux anomalies, which are due to the linearity assumption in the kernel, the assumption that the same proportion of cloud masking of the radiative forcing occurs in the A2 scenario as in a CO₂ doubling experiment in the GFDL model, and that this 16% masking is spatially uniform.

Generally, when compared with actual model-produced TOA radiation flux anomalies at the end of the 21st Century, the kernel predicts less LW cooling of the planet, though the opposite is

the case over specific regions in some models (not shown). In contrast, the actual model-produced downwelling SW flux anomalies are more positive than the kernel-derived SW flux anomalies nearly everywhere in every model. This feature is generally larger in the NH and especially over the continents, possibly indicating regional reductions in reflective aerosols that enhance the warming relative to what is predicted from using a spatially uniform SW radiative forcing in the kernel calculation. The GFDL models in particular exhibit the largest increase in actual absorbed SW radiation relative to what is predicted by the kernel (not shown), consistent with the large NH radiative forcing due to short-lived species shown in Figure 4 of Shindell et al. (2008).

5. Zonal-Mean Structure of Climate Feedbacks

In Figure 3 we show the zonal mean temperature, water vapor, cloud, and surface albedo feedbacks, along with the combined temperature-water vapor and sum of all feedbacks for the 12 models that archive enough data and for the multi-model mean. Water vapor feedback is greatest in the Tropics and declines from approximately $4 \text{ W m}^{-2} \text{ K}^{-1}$ at the equator to $1 \text{ W m}^{-2} \text{ K}^{-1}$ at the poles (Figure 3a). This gradient is almost completely offset at most latitudes by the temperature (Planck plus lapse rate) feedback, which is $-5 \text{ W m}^{-2} \text{ K}^{-1}$ in the Tropics and decreases monotonically to about $-2 \text{ W m}^{-2} \text{ K}^{-1}$ in the Antarctic (Figure 3b). Interesting hemispheric asymmetry is present in the temperature feedback due to the delayed warming in southern high latitudes and strong polar amplification of surface warming in the NH. The temperature feedback weakens to about $-3.5 \text{ W m}^{-2} \text{ K}^{-1}$ at 50°N , then strengthens to $-5 \text{ W m}^{-2} \text{ K}^{-1}$ over the north pole.

The net water vapor plus temperature feedback thus has a weak pole-to-pole gradient with a stronger negative feedback in the NH compared to the SH (Figure 3c). The hemispheric asymmetry

can be understood to zeroth order simply by considering geography: The SH has a little over twice as much ocean area as does the NH (c.f., Figure 1.12 of Hartmann (1994)) and a robust feature of GCM simulations is that the land heats up much more than the ocean by the end of the century (Meehl and Coauthors (2007)). The exact reason for this surface warming pattern, however, remains a subject of debate in the literature (e.g., Sutton et al. (2007); Joshi et al. (2008); Dong et al. (2009)). Certainly, vigorous vertical mixing in the Southern Ocean allows for large heat uptake and storage away from the surface, delaying the greenhouse gas-induced warming in this region.

The combined temperature and water vapor feedbacks exhibit significantly reduced inter-model spread at all latitudes than either feedback taken alone. Compensation of lapse rate and water vapor feedbacks is expected if relative humidity remains approximately constant (Cess (1975)) and is especially significant in the Tropics where temperature and humidity variations in the upper troposphere are large. Thus, models with strong negative lapse rate feedbacks (i.e., large tropical upper tropospheric warming) are also models with strong positive water vapor feedbacks such that the combination of the two feedbacks exhibits less inter-model spread than either taken alone (Soden and Held (2006)).

Net cloud feedback is positive (approximately $1 \text{ W m}^{-2} \text{ K}^{-1}$) between 45°N and 45°S and is negative in high latitudes (Figure 3d). As in the globally-integrated case, the inter-model spread in total feedback at each latitude is dominated by the inter-model spread in cloud feedback. In Figure 4 we separate the cloud feedback into its LW and SW components. It is clear that the SW cloud feedback uncertainties are much larger at all latitudes than the LW cloud feedback uncertainties. Furthermore, the LW cloud feedback is robustly positive across all models in the deep Tropics, and only a few models exhibit negative LW cloud feedbacks at any latitude. Zelinka and Hartmann (2010) showed that the robustly positive tropical LW cloud feedback is simply due to the fact that tropical high clouds rise as the climate warms, and that models capture this because it arises as a

fundamental result of radiative-convective equilibrium. Zelinka et al. (2011, manuscript submitted to *J. Climate*) show for a different ensemble of models that the positive LW cloud feedback at all latitudes – including the extratropics – is primarily caused by rising cloud tops. The deep Tropics experience the largest positive LW cloud feedback because the ensemble-mean SST and corresponding deep convection anomalies shift onto the equator in the A2 scenario in a pattern reminiscent of a permanent warm phase El Niño (Meehl and Coauthors (2007)).

A robust aspect of the SW cloud feedback structure is a transition from positive values to negative values in the extratropics, with a zero-crossing near 45° in both hemispheres. This is especially apparent in the more zonally-symmetric SH extratropics. Zelinka et al. (2011, manuscript submitted to *J. Climate*) demonstrate using a different ensemble of GCMs that this enhanced reflection is a manifestation of both the poleward shift of the midlatitude storm track and its attendant cloudiness as well as a brightening of clouds in sub-polar regions, the latter being the dominant contributor. However, Trenberth and Fasullo (2010) have shown that this robust Southern Ocean feature may be an artifact arising from cloud fraction biases in the mean state of the models, specifically, that the cloud cover is too small over the Southern Ocean in the mean, and therefore the increase in cloud cover and reflectivity is unrealistic.

The global average net feedback is $-1 \text{ W m}^{-2} \text{ K}^{-1}$. In the subtropics and extratropics the net feedback is about $-1.5 \text{ W m}^{-2} \text{ K}^{-1}$, with significant inter-model variance that is primarily attributable to variance in SW cloud feedback. Interestingly, the ensemble mean sum of all feedbacks is positive at the equator, indicating a climate that is locally unstable (Figure 3f). That is, as the planet warms due to long-lived greenhouse gas forcing, the atmospheric feedbacks act to increase the net radiative energy flux into the Tropics. This net positive feedback at the equator is due to a combination of weak net temperature plus water vapor feedback and strong positive LW cloud feedback. Both can be fundamentally explained by the exponential dependence of water vapor on

temperature through the Clausius Clapeyron relation and the strong dependence of radiative cooling on water vapor. The net negative feedbacks at high northern latitudes are a result of strong negative cloud feedbacks and, over the Arctic, increased emission to space due to the enhanced warming of the lower troposphere.

1) DISCUSSION

We consider several of the feedback response structures to be robust features of a warming climate that any model should capture regardless of parameterization. First, there are several reasons to expect an equator-to-pole gradient in the water vapor feedback:

- i. The sensitivity of OLR to water vapor perturbations (as indicated by the LW water vapor radiative kernel) is greatest in the tropical upper troposphere and decreases with latitude. Thus, the equator-to-pole gradient would exist even if increases in atmospheric moisture were spatially uniform.
- ii. The Clausius-Clapeyron relation exhibits a high sensitivity of saturation vapor pressure (e_s) to temperature at very cold temperatures and low pressures (e.g., e_s increases 15 % K^{-1} at 200 K compared to only 6 % K^{-1} at 300 K). Thus, even if temperature increased uniformly everywhere and relative humidity did not change, the largest fractional increase in absolute humidity would be in the tropical upper troposphere.
- iii. It is well accepted that tropical temperatures tend to follow the moist adiabat, resulting in upper tropospheric amplification of warming. Thus, assuming relative humidity is constant, enhanced moistening in the tropical upper troposphere would occur even in the absence of nonlinearities in the Clausius-Clapeyron relation.

Second, a robustly positive LW cloud feedback that is strongest in the Tropics is also expected from basic theoretical arguments, as it arises as a consequence of radiative-convective equilibrium (Hartmann and Larson (2002); Zelinka and Hartmann (2010)). A more negative cloud feedback in the high latitudes is an interesting feature that may be expected from basic principles, but a strong caution is provided by Trenberth and Fasullo (2010). That a dry model forced only with a rising extra-tropical tropopause produces a poleward-shifted jet and storm track (Lorenz and DeWeaver (2007)) implies that such features produced by GCMs (Hall et al. (1994); Yin (2005); Wu et al. (2010)) and the cloud anomalies that accompany them are believable. Furthermore, independent of any shift in the mean storm track and its attendant cloudiness, cloud optical properties have intrinsic temperature sensitivities that could plausibly cause a negative SW cloud feedback in extra-tropical latitudes as the planet warms (e.g., Feigelson (1978); Somerville and Remer (1984); Senior and Mitchell (1993); Tsushima et al. (2006)). Additionally, a warming atmosphere underlain by a less rapidly warming ocean may be expected to result in increased coverage of marine clouds (e.g., Klein and Hartmann (1993); Wood and Bretherton (2006))

Third, the factor of two difference in land fraction in the NH compared with the SH and the much larger capacity of the ocean to store heat compared with land implies that transient warming will be much less in southern mid- to high latitudes than in the north.

In the case of the mean state, regions of TOA energy surplus do not warm continuously while regions of energy deficit cool continuously; rather the atmosphere and oceans transport heat from surplus to deficit regions (e.g., Vonder Haar and Oort (1973); Trenberth and Solomon (1994); Trenberth and Caron (2001); Trenberth and Stepaniak (2003)). Anomalous meridional heat fluxes by the climate system perform the analogous role under global warming, diverging heat from regions in which feedbacks amplify the heating caused by greenhouse gas forcing and converging heat into regions in which feedbacks dampen the heating caused by greenhouse gas forcing. Thus

the structure of the net feedback requires an increase in the flux of energy from the equator to other latitudes by the climate system. Given the robust nature of the feedback structures discussed in this section, we can ascribe greater confidence to their implied anomalous poleward energy fluxes. This is explored in section 7.

6. Change in Surface Fluxes over the 21st Century

We now take a surface perspective and assess the change in surface fluxes between the end and the beginning of the 21st Century. This will allow for partitioning of the implied poleward heat transport between ocean and atmosphere, as atmospheric transport anomalies depend only on atmospheric net heating anomalies. Figure 5 shows the sensitivity of the surface fluxes to global mean temperature change. We have taken into account a surface cooling term caused by anomalous absorption of latent heat of fusion in the melting of snow but do not show it here, as it is a very small term at all latitudes. Note that positive values represent anomalous fluxes *into* the atmosphere. Transient warming is associated with a net increase in the flux of energy into the surface of about $0.4 \text{ W m}^{-2} \text{ K}^{-1}$, with generally larger fluxes into the surface at higher latitudes. One can think of this anomalous surface flux as a negative feedback on transient global warming. Ultimately, this term approaches zero as the climate equilibrates on the timescale of deep ocean mixing (Solomon et al. (2009)).

Changes in absorption of SW radiation by increased atmospheric water vapor as well as changes in SW cloud radiative forcing that accompany greenhouse warming result in a slight decrease in net SW heating of the surface, though with considerable inter-model spread (Figure 5a). An interesting feature is the consistent reduction in SW heating of the surface over the Southern Ocean.

Enhanced downwelling longwave radiation at the surface (i.e., LW cooling of the atmosphere;

not shown) increases more than does upwelling LW emission from the surface (not shown) with global temperature rise, though both increase dramatically and with very little inter-model spread (Figure 5b). Net LW fluxes actually cool the surface over many regions of the subtropical continents (not shown). Large anomalies in net atmospheric LW emission to the surface occur for almost every model at nearly every latitude, but especially in the warm, moist Tropics.

The net radiative flux anomaly at the surface is dominated by LW flux changes, as the “back radiation” from the atmosphere increases dramatically over the course of the century (Figure 5c). One notable exception is the Southern Ocean region, where SW flux changes due to clouds reduces the net heating of the surface over a narrow latitudinal band.

Enhanced radiative heating of the surface is almost completely compensated by an increase in evaporation (anomalously positive latent heat flux from surface to atmosphere) at almost every latitude (Figure 5d), though the inter-model variance in this flux is quite large. Anomalous latent heat fluxes are robustly negative in the Southern Ocean region, where the air-sea humidity gradient is reduced (Russell et al. (2006a)). The peak increase in latent heat flux to the atmosphere occurs at about 10°S in the ensemble mean, for reasons that remain to be investigated.

In the zonal mean, sensible heat flux anomalies are negative everywhere except over the poles, indicating that the atmosphere anomalously heats the surface at most latitudes as the planet warms (Figure 5e). However, the full spatial pattern (not shown) indicates that the sensible heat flux anomalies are into the atmosphere over continents, where the surface warms more than the atmosphere. Again, the Southern Ocean stands out as a prominent area of anomalous sensible heat transfer from atmosphere to ocean, though the NH midlatitudes and sub-polar latitudes also exhibit this feature to a lesser extent.

The general shape of the anomalous surface fluxes is characterized by a minimum in heat loss to the ocean in low latitudes that generally increases with latitude to large fluxes into the ocean in

sub-polar latitudes (Figure 5f). Thus the surface flux anomaly structure mimics that of the TOA flux anomaly, resulting in a preferential heating of the tropical atmosphere relative to the high latitudes. This has important implications for the partitioning of heat fluxes between ocean and atmosphere as the planet warms. Specifically, the atmosphere must perform more of the poleward heat transport than the ocean. This is discussed in greater detail in the next section.

A dominant feature in the net surface flux sensitivity is a net downward flux of energy of about $2 \text{ W m}^{-2} \text{ K}^{-1}$ that is concentrated in the southern extratropics. The largest part of this comes from the net downward flux of sensible heat from the atmosphere to the surface, but the net downward flux of latent heat and LW radiation also contribute. The Southern Ocean feature is present in all the models, though with different magnitudes and latitudes of peak heat uptake. This feature makes physical sense considering the vigorous vertical oceanic mixing that brings cold water to the surface and facilitates anomalous sensible heat transfer from atmosphere to ocean.

7. Poleward Energy Flux Sensitivity to Feedback Processes

We have shown that the radiative kernel allows one to decompose the change in net TOA radiation at every location into the individual components causing the change. Here we take the latitudinal structure of each component's radiation anomaly and calculate its implied poleward energy transport anomaly. This is done using a polar cap integration in which the anomalous energy flux across a latitude circle is equal to the TOA radiation anomaly within the polar cap extending to that latitude (c.f. Eqn. 2.21 of Hartmann (1994)):

$$F'(\phi) = \int_{-\frac{\pi}{2}}^{\phi} \int_0^{2\pi} R' a^2 \cos\phi d\lambda d\phi, \quad (3)$$

where $F'(\phi)$ is the anomalous northward energy flux across a latitude circle, ϕ is latitude, λ is longitude, a is the radius of the Earth, and R' is the anomalous TOA radiation anomaly with its global mean value subtracted out. Negative anomalous net integrated TOA radiation within the polar cap (i.e., a net energy deficit anomaly at the TOA) implies an anomalous poleward flux of energy across the latitude circle into the cap. This same equation can be used to calculate the required poleward energy flux due to the latitudinal gradients in TOA radiative flux anomaly associated with each individual feedback component (temperature, water vapor, surface albedo, and clouds). In the case of transient global warming, the feedback processes discussed above have latitudinal gradients that individually impact the implied poleward heat flux.

We can also partition the net poleward heat transport between the atmosphere and ocean by taking into account the anomalous surface fluxes that accompany transient warming (discussed in the previous section). The implied atmospheric poleward transport is simply given as

$$F'_{atm}(\phi) = \int_{-\frac{\pi}{2}}^{\phi} \int_0^{2\pi} (R' + F'_{sfc}) a^2 \cos\phi d\lambda d\phi, \quad (4)$$

where $F'_{atm}(\phi)$ is the anomalous northward atmospheric energy flux across a latitude circle and F'_{sfc} is the anomalous surface flux anomaly with its global mean value subtracted out. In Figure 6 we plot the anomalous poleward transports that are implied by each feedback process and by the change in surface fluxes over the course of the century.

Taken alone, atmospheric and surface temperature anomalies that accompany global warming result in a huge radiative loss of energy to space in the Tropics and at high northern latitudes (Figure 3a). This requires anomalous northward heat flux by the climate system at nearly every latitude, implying that such a warming structure requires net flux from the SH to the NH (Figure 6a). Massive heat flux convergence into the Tropics is required due to anomalous emission from

the warmer upper troposphere.

Water vapor feedback, which acts to preferentially heat the Tropics, implies a nearly hemispherically symmetric anomalous poleward heat flux that diverges heat from the deep Tropics (Figure 6b). This strongly opposes the anomalous heat flux convergence into the Tropics that is implied by the temperature feedback.

Implied anomalous transport due to the cloud feedback exhibits considerable spread, but is generally symmetric about the equator, requiring poleward flux in each hemisphere (Figure 6d). Unlike the water vapor feedback, which decreases roughly monotonically with latitude, the cloud feedback remains positive until about 50° in either hemisphere, at which point it exhibits a rather sharp drop-off with latitude (Figure 3d). This results in an anomalous poleward transport due to clouds that peaks at higher latitudes than does the transport due to water vapor. Weaver (2003) speculated that changes in extratropical cloud radiative forcing that accompany storm track shifts in a warm climate could have a large influence on poleward heat flux; here we show that cloud changes do indeed require enhanced poleward heat flux.

Surface albedo feedbacks require reduced poleward heat flux in each hemisphere, but are much smaller at nearly every latitude than other individual implied transports (Figure 6e). This is a slightly counterintuitive result, considering that one might expect the albedo feedback to be associated with enhanced flux of heat to the poles, where it can go into melting snow and ice. However, we are showing here the poleward heat flux anomalies due to albedo feedback alone, which preferentially heats the poles and implies a requirement for less heat flux into the polar area.

In a similar manner to the implied transport due to clouds and water vapor feedbacks, the anomalous surface fluxes require enhanced poleward transport by the atmosphere. Because the atmosphere warms faster than the ocean at high latitudes, the ocean provides less heat to the atmosphere in high latitudes and the atmosphere must carry more heat poleward (Figure 6c). In

other words, the latitudinal structure of anomalous surface fluxes tends to amplify the latitudinal structure of TOA radiative fluxes, thereby requiring the atmosphere to transport more heat in a warming climate.

Figure 7a shows the model ensemble average TOA flux anomalies with the global mean removed, and Figure 7b shows the meridional flux anomalies required by the gradients TOA flux anomalies. The net radiative plus surface flux shows a peak positive anomaly in the equatorial region, as already noted, that requires an enhanced meridional flux away from the equator. The primary contributors to this equatorial peak are water vapor and longwave cloud feedbacks. Other notable features are the large transitions from net positive atmospheric heating anomalies on the equatorial side of the midlatitudes to net negative atmospheric heating anomalies on the poleward side of the midlatitudes. In both hemispheres, the midlatitude cooling anomaly is about twice as large as the heating anomaly, and the magnitude of this latitudinal fluctuation is about twice as large in the SH than in the NH. These are caused by the combination of strong negative cloud feedbacks and large anomalous fluxes of heat into the ocean. It is interesting that the subpolar atmosphere loses heat both out of its top by way of strong negative cloud feedbacks as well as out of its bottom by way of strong sensible and longwave fluxes to the surface. This feature is larger in the SH because the cloud feedback and anomalous surface flux signatures are more sharply defined and co-located than their NH counterparts, and because the opposing positive surface albedo feedback extends farther equatorward in the NH. Required poleward flux anomalies reflect these midlatitude features, exhibiting secondary peaks in the midlatitudes such that narrow latitude bands experience heat flux divergence while the poles receive enhanced heat flux convergence.

The temperature feedback shows a strong hemispheric asymmetry with more positive values (relative to the global mean) in the SH than in the NH. The temperature feedback asymmetry is, as always, offset somewhat by the water vapor feedback. On the equator, however, the northward

energy flux change associated with temperature is partially offset equally by water vapor, cloud and surface albedo feedbacks, leaving a small residual northward net flux change. This net northward heat flux at the equator must be accomplished by anomalous northward dry static energy transport by a southward-shifted Hadley Circulation (Kang et al. (2008), Kang et al. (2009)). In each hemisphere, the peak poleward heat flux anomalies are roughly 0.8 PW per degree of global mean temperature increase. Considering the global warming simulated by the models is 3.5 K, these flux changes are as large as 20% of the mean atmospheric flux in low- and mid-latitudes (c.f., Figure 2.14 of Hartmann (1994)).

Ensemble mean implied poleward heat transport anomalies in the climate system are shown in Figure 8. The “ocean” term is not the change in poleward oceanic heat flux, but rather the sum of the change in oceanic poleward flux and heat storage computed by assuming all net surface fluxes into the surface go into either storage or transport in the ocean. Also shown is the poleward heat transport anomaly computed using the ensemble mean TOA flux anomalies produced by the models (i.e., archived directly by the model rather than implied from the radiative kernel calculation).

Clearly there are differences between the implied poleward fluxes estimated using the kernel technique and derived directly from the models’ TOA fluxes, especially in the NH. This can be attributed to the uncertainties in G discussed earlier. The kernel-derived fluxes imply more (less) poleward transport in low (high) latitudes of the NH than the directly-computed TOA flux anomalies. In the ensemble mean, actual TOA SW anomalies are more positive than those computed with the kernel over the majority of the NH, especially in midlatitudes, and much more negative over the Arctic than those computed with the kernel, possibly indicating a strong local reduction of reflective aerosols in the midlatitudes that is not captured by our simple use of \overline{G} . In the ensemble mean, the actual TOA LW anomalies are more negative at the equator and pole and more positive in midlatitudes than those computed with the kernels. It is unclear why this structure emerges,

but may also be related to changes in absorbing aerosol that are very regionally-dependent. Such unaccounted-for anomalous heating of NH midlatitudes relative to the Tropics and poles would require less poleward flux at low latitudes and more poleward flux at high latitudes, which is what we see when comparing the solid and dashed red curves. Obviously uncertainties in aerosol forcing strongly impact the implied anomalous poleward heat flux that accompanies global warming.

Regardless of the details of the aerosol forcing, it is clear from this figure that oceanic poleward heat transport and storage anomalies act in the opposite sense to what is required at the TOA, thereby placing more of the burden of transporting heat to the pole on the atmosphere. Furthermore, hemispheric asymmetry in the net TOA flux anomalies results in hemispheric asymmetry in the implied anomalous poleward heat transports, with an additional $1.2 \times 10^{13} \text{ W K}^{-1}$ heat transported northward by the climate system. (Relative to the global mean, the NH loses an anomalous $0.06 \text{ W m}^{-2} \text{ K}^{-1}$ to space while the SH gains an additional $0.06 \text{ W m}^{-2} \text{ K}^{-1}$.)

Several important conclusions are drawn from this section. First, poleward heat transport in a warming climate is enhanced due to the presence of feedbacks (e.g., Wu et al. (2010)). Second, feedbacks that may be considered “local” from the TOA perspective have relevance at all latitudes due to their induced circulation responses (e.g., Chiang and Bitz (2005), Yoshimori and Broccoli (2008), Kang et al. (2008), Kang et al. (2009), Fletcher et al. (2009), Hwang and Frierson (2010)). Third, locally large positive feedbacks need not imply locally large surface temperature changes if compensated by anomalous horizontal heat flux divergence. Finally, the atmosphere must perform more of the net poleward heat transport in the presence of an underlying ocean (e.g., Held and Soden (2006)).

8. Summary, Discussion, and Implications

Positive feedbacks in the climate system act to reduce the efficiency with which the planet comes back into radiative equilibrium following a sustained radiative forcing due to long-lived greenhouse gases. This results in a planet that must warm more than if there were no amplifying feedbacks present. We have shown in this paper that these feedbacks have rich spatial structures that – by conservation of energy – have implications on poleward heat transport in a warming climate. In general, a warming planet is associated with feedbacks that act to preferentially heat the Tropics relative to the poles, effectively strengthening the mean state equator-to-pole energy gradient and requiring the climate system to transport more heat poleward, in agreement with previous studies (e.g., Wu et al. (2010), Hwang and Frierson (2010)).

A particular strength of this study is the use of radiative kernels to partition the net feedback and its implied poleward heat transport anomalies among its individual components. In so doing, we have shown that enhanced poleward heat transport is necessitated by the decrease with latitude of water vapor and cloud feedbacks. Furthermore, we can attribute most of the uncertainty in poleward heat flux changes to uncertainties in the SW cloud feedback, a result also found by Hwang and Frierson (2010). Interestingly, changes in the LW radiative budget of the planet under global warming necessitate enhanced northward flux in both hemispheres whereas changes in the SW radiative budget of the planet necessitate enhanced southward flux in both hemispheres.

Net TOA radiative loss is greater by the end of the century in the NH than in the SH, resulting in a hemispheric gradient in net radiation anomaly that must be balanced by a general increase in flux from south to north as the planet warms, as occurs in idealized experiments with hemispherically-asymmetric heating (e.g., Kang et al. (2008)). In the Tropics this is most likely accomplished by enhanced northward flux by a southward-shifted Hadley circulation. In the midlatitudes this must be accomplished by stronger and poleward-shifted eddies (e.g., Hall et al. (1994), Wu et al. (2010)).

The ocean has tremendous thermal inertia in high latitudes, where the ocean mixes to depth and can access the huge heat capacity of the deep ocean. This impedes the warming of the upper ocean in high latitudes relative to other latitudes and facilitates large anomalous surface heat fluxes out of the high latitude atmosphere as the planet warms. The surface flux anomalies amplify the latitudinal gradient of heat loss from the atmosphere and require that the atmosphere perform more of the poleward heat transport and the ocean less.

We have argued that several of the gross features of the climate response can be expected from basic principles, namely that the water vapor feedback exhibit a maximum at low latitudes where OLR is most sensitive to water vapor perturbations and where the greatest moistening occurs, that the cloud feedback be positive at low latitudes due to the rising of tropical cloud tops and negative at high latitudes due to a shifted storm track and/or a brightening of clouds (due to increased liquid water content), that LW emission from the NH be larger than that from the SH because of the hemispheric gradient in surface warming that can largely be attributed to continental geography (i.e., twice as much ocean in the SH), and that anomalous oceanic heat uptake preferentially occur at high latitudes, where vigorous mixing and deep water formation are most efficient. In sum, these features give us confidence that a robust increase in poleward heat transport by the climate system, with atmospheric transport increasing at the expense of oceanic transport, is realistic and makes sense intuitively.

Finally, this study has illuminated several interesting features of the climate system.

Horizontal heat transport, radiative heating, and surface warming are intimately coupled such that regions that are anomalously heated by radiation (i.e., by forcings and feedbacks) are anomalously cooled by dynamics (i.e., by meridional heat transport). Thus one can think of dynamical heating as a negative feedback on radiative heating at local scales. This is an important result that implies – for example – that models with large surface albedo feedbacks need not be models having

large anomalous heat flux convergence into the high latitudes, a point also made by Hwang and Frierson (2010).

It is also noteworthy that although each feedback has particular regions in which it is most pronounced (e.g., over the poles for surface albedo feedback), it impacts the implied poleward transport at all latitudes. Thus, processes occurring in remote regions of the planet influence the energy budget throughout the climate system, even if they are not important (from a TOA perspective) locally. This point was emphasized by Fletcher et al. (2009) in the response of atmospheric circulation to snow albedo feedback on NH land as well as by Chiang and Bitz (2005), Yoshimori and Broccoli (2008), Kang et al. (2008), and Kang et al. (2009) in the movement of the ITCZ due to extratropical forcings. Kang et al. (2009) additionally showed that cloud and water vapor feedbacks cause a larger atmospheric response to hemispherically-asymmetric imposed radiative forcing than in an idealized model (Frierson et al. (2006)) in which those feedbacks are suppressed, a result consistent with our findings.

Another point that is perhaps unappreciated is that anomalies in meridional heat transport depend on latitudinal anomalies of feedbacks from their global mean values rather than the magnitudes of their global mean values. It thus follows that feedbacks that are relatively unimportant for climate sensitivity because they globally integrate to a small number can hypothetically be very important for anomalous heat transport. This is obvious from the results of Kang et al. (2008) and Kang et al. (2009), who showed that a hemispherically asymmetric radiative forcing anomaly that integrated to zero globally caused large changes in poleward heat flux. Although we find in this study that the largest individual contributors to anomalous heat transport tend to also be the largest globally-integrated feedbacks, it is interesting to recognize that this need not be the case.

Finally, the Southern Ocean region, in which the atmosphere and ocean strongly influence each other, stands out in this study as one in which the transient response of the climate is

dramatic. Russell et al. (2006b), Russell et al. (2006a), Delworth and Zeng (2008), Toggweiler and Russell (2008), and Sen Gupta et al. (2009)) have emphasized the importance of surface westerlies over the Southern Ocean as well as their poleward shift and intensification in allowing for increased oceanic heat uptake in the face of increased upper ocean stratification during transient warming. They find that the inter-model spread in Southern Ocean heat uptake is in large part attributable to the response of surface westerlies in this region, which themselves are likely to be affected both in strength and location by the requirements of poleward heat transport set in place by TOA and surface flux anomalies. Caution is, however, provided by Boning et al. (2008) and Farneti and Delworth (2010), who suggest that the large sensitivity of Southern Ocean circulation to surface winds may be exaggerated in coarse resolution ocean models that do not resolve eddies. Regardless, one could conceive of possible feedbacks (in the generic sense) involving a poleward-shifted storm track, the latitudinal gradient of cloud feedbacks, the strength of the surface winds over the Southern Ocean, upwelling and attendant heat uptake in the Southern Ocean, and meridional temperature gradients, all of which likely interact with one another in ways that – to our knowledge – have not been adequately explored. The Southern Ocean’s importance in taking up both heat and anthropogenic CO₂ (Mignone et al. (2006)) argues for more extensive investigation into such regional feedbacks.

Acknowledgments.

This research was supported by NASA Grant NNX09AH73G, NASA Earth and Space Science Fellowship NNX06AF69H, and by the Lawrence Livermore National Laboratory Institutional Postdoc Program. We acknowledge the international modeling groups for providing their data for analysis, the Program for Climate Model Diagnosis and Intercomparison (PCMDI) for collecting and archiving the model data, and B. J. Soden for providing the radiative kernels. We thank

Dargan Frierson, Yen-Ting Hwang, Angie Pendergrass, Kyle Armour, Aaron Donohoe, and Chris Bretherton for useful discussion and suggestions for improvement, as well as Marc Michelsen for computer support. This work performed under the auspices of the U.S. Department of Energy by Lawrence Livermore National Laboratory under Contract DE-AC52-07NA27344.

REFERENCES

- Boning, C. W., A. Dispert, M. Visbeck, S. R. Rintoul, and F. U. Schwarzkopf, 2008: The response of the Antarctic Circumpolar Current to recent climate change. *Nature*.
- Cess, R. D., 1975: Global climate change - investigation of atmospheric feedback mechanisms. *Tellus*, **27** (3), 193–198.
- Chiang, J. C. H. and C. M. Bitz, 2005: The influence of high latitude ice on the position of the marine Intertropical Convergence Zone. *Climate Dyn.*, doi:10.1007/s00382-005-0040-5.
- Colman, R., 2003: A comparison of climate feedbacks in general circulation models. *Climate Dyn.*, **20**, 865–873.
- Delworth, T. L. and F. Zeng, 2008: Simulated impact of altered southern hemisphere winds on the Atlantic Meridional Overturning Circulation. *Geophys. Res. Lett.*, **35**, L20708, doi:10.1029/2008GL035166.
- Dong, B., J. M. Gregory, and R. T. Sutton, 2009: Understanding land-sea warming contrast in response to increasing greenhouse gases. Part I: Transient adjustment. *Journal of Climate*, **22** (11), 3079–3097.
- Farneti, R. and T. L. Delworth, 2010: The role of mesoscale eddies in the remote oceanic response to altered Southern Hemisphere winds. *J. Phys. Oceanogr.*, **40** (10), 2348–2354.
- Feigelson, E. M., 1978: Preliminary radiation model of a cloudy atmosphere. Part I: Structure of clouds and solar radiation. *Beitr. Phys. Atmos.*, **51**, 203–229.

- Fletcher, C. G., P. J. Kushner, A. Hall, and X. Qu, 2009: Circulation responses to snow albedo feedback in climate change. *Geophys. Res. Lett.*, **36**, L09702, doi:10.1029/2009GL038011.
- Frierson, D. M. W., I. M. Held, and P. Zurita-Gotor, 2006: A gray-radiation aquaplanet moist GCM. Part I: Static stability and eddy scale. *Journal of the Atmospheric Sciences*, **63** (10), 2548–2566.
- Hall, N. M. J., B. J. Hoskins, P. J. Valdes, and C. A. Senior, 1994: Storm tracks in a high-resolution gcm with doubled carbon dioxide. *Quart J Roy Meteorol Soc*, **120**, 1209–1230.
- Hansen, J., A. Lacis, D. Rind, G. Russell, P. Stone, I. Fung, R. Ruedy, and J. Lerner, 1984: Climate processes and climate sensitivity: Analysis of feedback mechanisms. *Geophys. Monogr.*, **29**, 130–163.
- Hartmann, D. L., 1994: *Global physical climatology*. Academic Press.
- Hartmann, D. L. and K. Larson, 2002: An important constraint on tropical cloud-climate feedback. *Geophys. Res. Lett.*, **29** (20), doi:10.1029/2002GL015835.
- Held, I. M. and B. J. Soden, 2006: Robust responses of the hydrological cycle to global warming. *J. Climate*, **19**, 5686–5699.
- Hwang, Y. T. and D. M. W. Frierson, 2010: Increasing atmospheric poleward energy transport with global warming. *Geophys. Res. Lett.*, **37**, L24807, doi:10.1029/2010GL045440.
- Joshi, M., J. Gregory, M. Webb, D. Sexton, and T. Johns, 2008: Mechanisms for the land/sea warming contrast exhibited by simulations of climate change. *Climate Dynamics*, **30**, 455–465.
- Kang, S. M., D. M. W. Frierson, and I. M. Held, 2009: The tropical response to extratropical thermal forcing in an idealized GCM: The importance of radiative feedbacks and convective parameterization. *Journal of the Atmospheric Sciences*, **66** (9), 2812–2827.

- Kang, S. M., I. M. Held, D. M. W. Frierson, and M. Zhao, 2008: The response of the ITCZ to extratropical thermal forcing: Idealized slab-ocean experiments with a GCM. *Journal of Climate*, **21** (14), 3521–3532.
- Klein, S. A. and D. L. Hartmann, 1993: The seasonal cycle of low stratiform clouds. *J. Climate*, **6**, 1587–1606.
- Lorenz, D. J. and E. T. DeWeaver, 2007: Tropopause height and zonal wind response to global warming in the IPCC scenario integrations. *J. Geophys. Res.*, **112**, D10119, doi:10.1029/2006JD008087.
- Meehl, G. A. and Coauthors, 2007: Global climate projections. *Climate Change 2007: The Physical Science Basis*, S. S. et al., Ed., Cambridge University Press, 747–846.
- Mignone, B. K., A. Gnanadesikan, J. L. Sarmiento, and R. D. Slater, 2006: Central role of Southern Hemisphere winds and eddies in modulating the oceanic uptake of anthropogenic carbon. *Geophys. Res. Lett.*, **33**, L01604, doi:10.1029/2005GL024464.
- Ramaswamy, V. et al., 2001: Radiative forcing of climate change. *Climate Change 2001: The Scientific Basis*, J. T. H. et al., Ed., Cambridge University Press, 350–416.
- Roe, G. H., 2009: Feedbacks, timescales, and seeing red. *Annual Reviews of Earth Plan. Sci.*, **37**, 93–115.
- Roe, G. H. and M. B. Baker, 2007: Why is climate sensitivity so unpredictable? *Science*, **318**, 629–632.
- Russell, J. L., K. W. Dixon, A. Gnanadesikan, R. J. Stouffer, and J. R. Toggweiler, 2006a: The Southern Hemisphere westerlies in a warming world: Propping open the door to the deep ocean. *J. Climate*, **19** (24), 6382–6390.

- Russell, J. L., R. J. Souffer, and K. W. Dixon, 2006b: Intercomparison of the Southern Ocean circulations in the IPCC coupled model control simulations. *J. Climate*, **19** (18), 4560–4575.
- Sen Gupta, A., A. Santoso, A. S. Taschetto, C. C. Ummenhofer, J. Trevena, and M. H. England, 2009: Projected changes to the Southern Hemisphere ocean and sea ice in the IPCC AR4 climate models. *J. Climate*, **22** (11), 3047–3078.
- Senior, C. and J. Mitchell, 1993: Carbon dioxide and climate. The impact of cloud parameterization. *J. Climate*, **6**, 393–418.
- Shindell, D. T., H. Levy, M. D. Schwarzkopf, L. W. Horowitz, J.-F. Lamarque, and G. Faluvegi, 2008: Multimodel projections of climate change from short-lived emissions due to human activities. *J. Geophys. Res.*, **113**, D11109, doi:10.1029/2007JD009152.
- Soden, B. J. and I. M. Held, 2006: An assessment of climate feedbacks in coupled ocean-atmosphere models. *J. Climate*, **19**, 3354–3360.
- Soden, B. J., I. M. Held, R. Colman, K. M. Shell, J. T. Kiehl, and C. A. Shields, 2008: Quantifying climate feedbacks using radiative kernels. *J. Climate*, **21**, 3504–3520.
- Solomon, S., G.-K. Plattner, R. Knutti, and P. Friedlingsteind, 2009: Irreversible climate change due to carbon dioxide emissions. **106** (6), 1704–1709.
- Somerville, R. C. J. and L. A. Remer, 1984: Cloud optical thickness feedbacks in the CO₂ climate problem. *J. Geophys. Res.*, **89** (D6), 9668–9672.
- Sutton, R. T., B. Dong, and J. M. Gregory, 2007: Land/sea warming ratio in response to climate change: IPCC AR4 model results and comparison with observations. *Geophys. Res. Lett.*, **34**, L02701, doi:10.1029/2006GL028164.

- Toggweiler, J. R. and J. Russell, 2008: Ocean circulation in a warming climate. *Nature*, **451**, 286–288.
- Trenberth, K. E. and J. M. Caron, 2001: Estimates of meridional atmosphere and ocean heat transports. *J. Climate*, **14 (16)**, 3433–3443.
- Trenberth, K. E. and J. T. Fasullo, 2010: Simulation of present-day and twenty-first-century energy budgets of the southern oceans. *Journal of Climate*, **23 (2)**, 440–454.
- Trenberth, K. E. and A. Solomon, 1994: The global heat balance: Heat transports in the atmosphere and ocean. *Climate Dyn.*, **10**, 107–134.
- Trenberth, K. E. and D. P. Stepaniak, 2003: Seamless poleward atmospheric energy transports and implications for the Hadley circulation. *J. Climate*, **16**, 3706–3722.
- Tsushima, Y., et al., 2006: Importance of the mixed-phase cloud distribution in the control climate for assessing the response of clouds to carbon dioxide increase: A multi-model study. *Climate Dyn.*, **27**, 113–126.
- Vonder Haar, T. H. and A. H. Oort, 1973: New estimate of annual poleward energy transports by Northern Hemisphere oceans. *J. Phys. Oceanogr.*, **3**, 169–172.
- Weaver, C. P., 2003: Efficiency of storm tracks an important climate parameter? The role of cloud radiative forcing in poleward heat transport. *J. Geophys. Res.*, **108**, doi:10.1029/2002JD002756.
- Wood, R. and C. S. Bretherton, 2006: On the relationship between stratiform low cloud cover and lower-tropospheric stability. *Journal of Climate*, **19 (24)**, 6425–6432.
- Wu, Y., M. Ting, R. Seager, H.-P. Huang, and M. Cane, 2010: Changes in storm tracks and energy transports in a warmer climate simulated by the GFDL CM2.1 model. *Climate Dyn.*, 1–20, doi:10.1007/s00382-010-0776-4.

Yin, J. H., 2005: A consistent poleward shift of the storm tracks in simulations of 21st century climate. *Geophys. Res. Lett.*, **32**, L18701, doi:10.1029/2005GL023684.

Yoshimori, M. and A. J. Broccoli, 2008: Equilibrium response of an atmosphere-mixed layer ocean model to different radiative forcing agents: Global and zonal mean response. *Journal of Climate*, **21** (17), 4399–4423.

Zelinka, M. D. and D. L. Hartmann, 2010: Why is longwave cloud feedback positive? *J. Geophys. Res.*, **115**, D16117, doi:10.1029/2010JD013817.

List of Tables

- 1 Global climate models that simulated the SRES A2 scenario and submitted sufficient data to the CMIP3 archive to permit computation of feedbacks using radiative kernels. Also shown in the comments are the relevant diagnostics not provided by each modeling center (if applicable). Cloud feedbacks cannot be computed with the radiative kernel without TOA clear-sky fluxes. Partitioning of poleward heat transport between ocean and atmosphere cannot be performed without surface fluxes. 35

TABLE 1. Global climate models that simulated the SRES A2 scenario and submitted sufficient data to the CMIP3 archive to permit computation of feedbacks using radiative kernels. Also shown in the comments are the relevant diagnostics not provided by each modeling center (if applicable). Cloud feedbacks cannot be computed with the radiative kernel without TOA clear-sky fluxes. Partitioning of poleward heat transport between ocean and atmosphere cannot be performed without surface fluxes.

Abbreviation	Modeling Center (Country)	Comment
ipsl_cm4	Institut Pierre Simon Laplace (France)	All fluxes provided
mpi_echam5	Max Planck Institute for Meteorology (Germany)	All fluxes provided
cccma_cgcm3_1	Canadian Centre for Climate Modelling & Analysis (Canada)	All fluxes provided
mri_cgcm2_3_2a	Meteorological Research Institute (Japan)	All fluxes provided
ukmo_hadcm3	Hadley Centre for Climate Prediction and Research / Met Office (U.K.)	All fluxes provided
gfdl_cm2_0	US Dept. of Commerce / NOAA / Geophysical Fluid Dynamics Laboratory (U.S.A.)	All fluxes provided
inmcm3_0	Institute for Numerical Mathematics (Russia)	All fluxes provided
miroc3_2_medres	Center for Climate System Research (The University of Tokyo), National Institute for Environmental Studies, and Frontier Research Center for Global Change (Japan)	All fluxes provided
ncar_ccsm3_0	National Center for Atmospheric Research (U.S.A.)	All fluxes provided
gfdl_cm2_1	US Dept. of Commerce / NOAA / Geophysical Fluid Dynamics Laboratory (U.S.A.)	All TOA fluxes but no SFC latent heat flux provided
ncar_pcm1	National Center for Atmospheric Research (U.S.A.)	All TOA fluxes but no SFC upwelling LW flux provided
giss_model_e_r	NASA / Goddard Institute for Space Studies (U.S.A.)	All TOA fluxes but no SFC LW fluxes over land provided
bccr_bcm2_0	Bjerknes Centre for Climate Research (Norway)	No TOA clear-sky fluxes provided
csiro_mk3_5	Commonwealth Scientific and Industrial Research Organization Atmospheric Research (Australia)	No TOA clear-sky upwelling SW flux provided
ingv_echam4	National Institute of Geophysics and Volcanology (Italy)	No TOA clear-sky fluxes or SFC radiative fluxes provided

List of Figures

- 1 Ensemble mean temperature, water vapor, cloud, and surface albedo feedbacks, along with the combined temperature-water vapor feedback and the sum of all feedbacks computed using the kernel technique. Note that the color scales vary among panels. 38
- 2 Ensemble mean LW, SW, and net cloud feedbacks computed by adjusting the change in cloud radiative forcings as described in the text. 39
- 3 Zonal mean (a) temperature, (b) water vapor, (c) combined temperature-water vapor, (d) cloud, and (e) surface albedo feedbacks, along with (f) the sum of all feedbacks. Each of the twelve models is represented by an individual gray line, and the thick black line represents the multi-model mean. The abscissa is sine of latitude so that the visual integral is proportional to Watts per Kelvin of mean surface temperature change. Note that the vertical axis limits vary among panels, but all span a range of $6 \text{ W m}^{-2} \text{ K}^{-1}$. 40
- 4 As in Figure 3 but for the (a) LW, (b) SW, and (c) net cloud feedbacks. Note that the vertical axis limits vary among panels, but all span a range of $7 \text{ W m}^{-2} \text{ K}^{-1}$. 41
- 5 Changes in surface (a) SW radiation, (b) LW radiation, (c) net radiation, (d) latent heat flux, and (e) sensible heat flux, along with (f) the sum of all terms over the 21st Century, expressed per unit of global mean temperature change. Positive anomalies represent anomalous fluxes *into* the atmosphere. Note that the vertical axis limits vary among panels, but all span a range of $6 \text{ W m}^{-2} \text{ K}^{-1}$. 42

- 6 Implied northward meridional heat flux anomalies in the climate system due to (a) temperature, (b) water vapor, (d) cloud, and (e) surface albedo feedbacks, and the implied *atmospheric* northward heat flux anomaly due to (c) anomalous surface fluxes and (f) the sum of TOA and surface heat flux anomalies. The implied northward energy fluxes are computed by integrating the TOA or surface flux anomalies over a polar cap as described in the text. 43
- 7 (a) Multi-model mean TOA and surface flux anomalies and (b) implied northward meridional heat flux anomalies due to changes in (red) temperature, (solid blue) water vapor, (thin black) surface albedo, (green) clouds, (dashed blue) surface fluxes, and (thick black) net fluxes into the atmosphere. The TOA and surface flux anomalies are plotted as anomalies from their global means. The implied northward energy fluxes are computed by integrating the TOA net flux anomalies over a polar cap as described in the text. 44
- 8 The implied changes in (red solid) net poleward transport by the climate system, partitioned into components due to changes in (black) atmosphere poleward transport and (blue) the sum of oceanic transport and storage. Also provided in the red dashed line is the net transport anomaly computed directly from the ensemble mean TOA flux anomalies (i.e., without use of the radiative kernels). Note that the black curve is the same as in Figure 7. 45

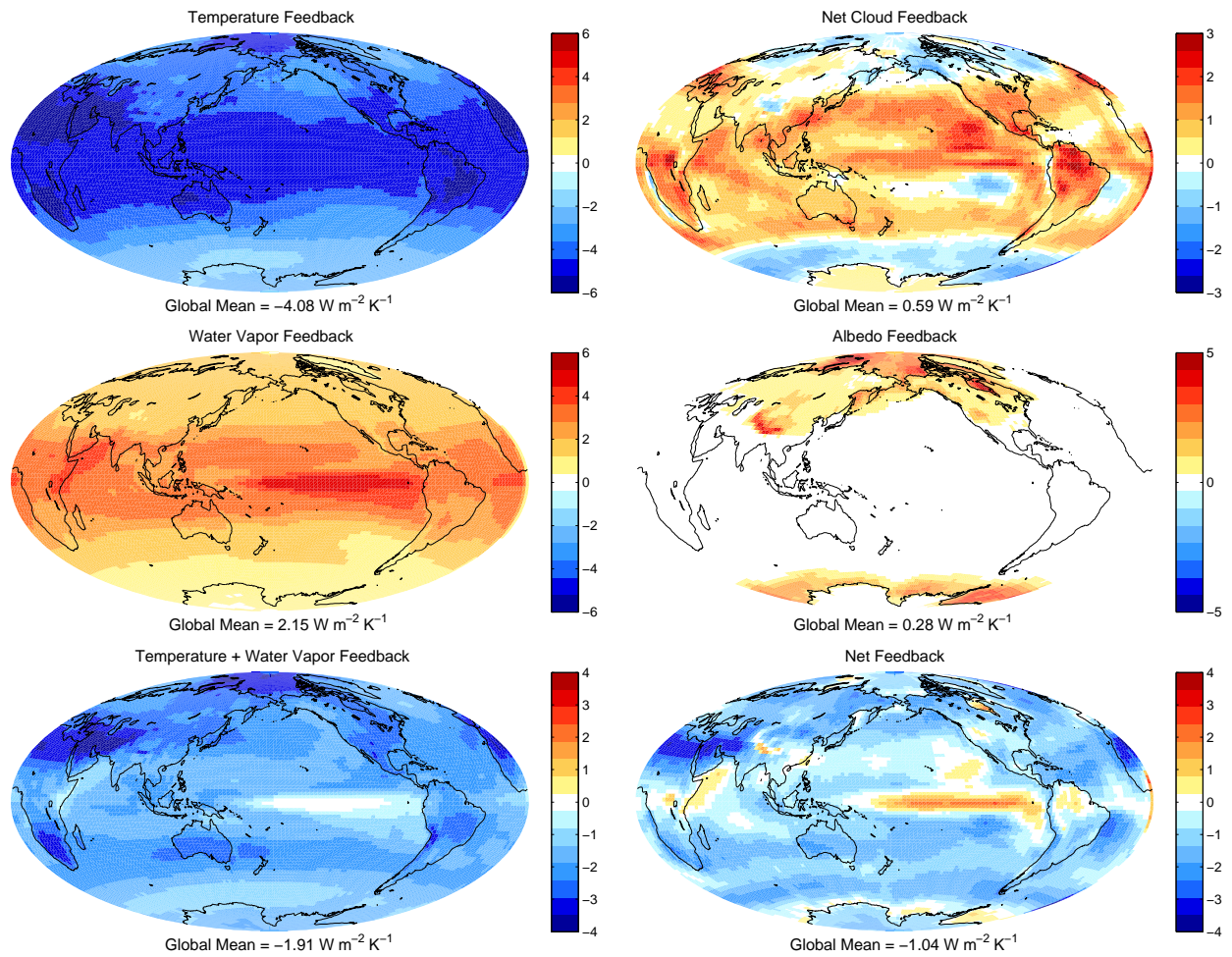


FIG. 1. Ensemble mean temperature, water vapor, cloud, and surface albedo feedbacks, along with the combined temperature-water vapor feedback and the sum of all feedbacks computed using the kernel technique. Note that the color scales vary among panels.

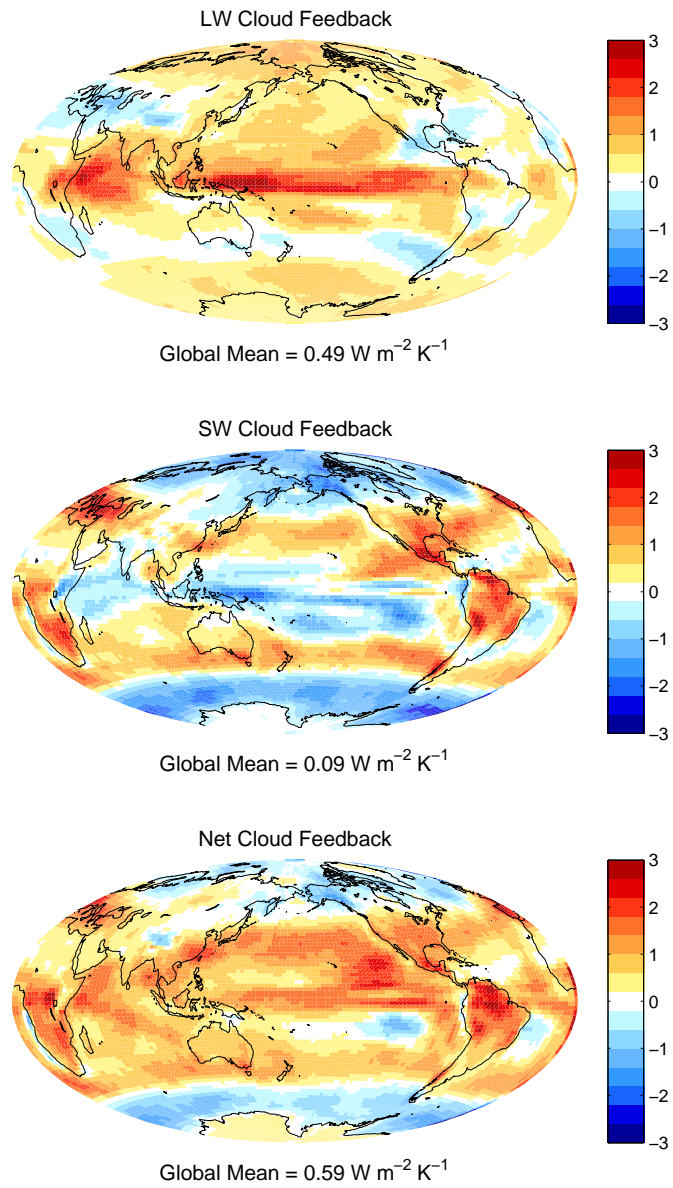


FIG. 2. Ensemble mean LW, SW, and net cloud feedbacks computed by adjusting the change in cloud radiative forcings as described in the text.

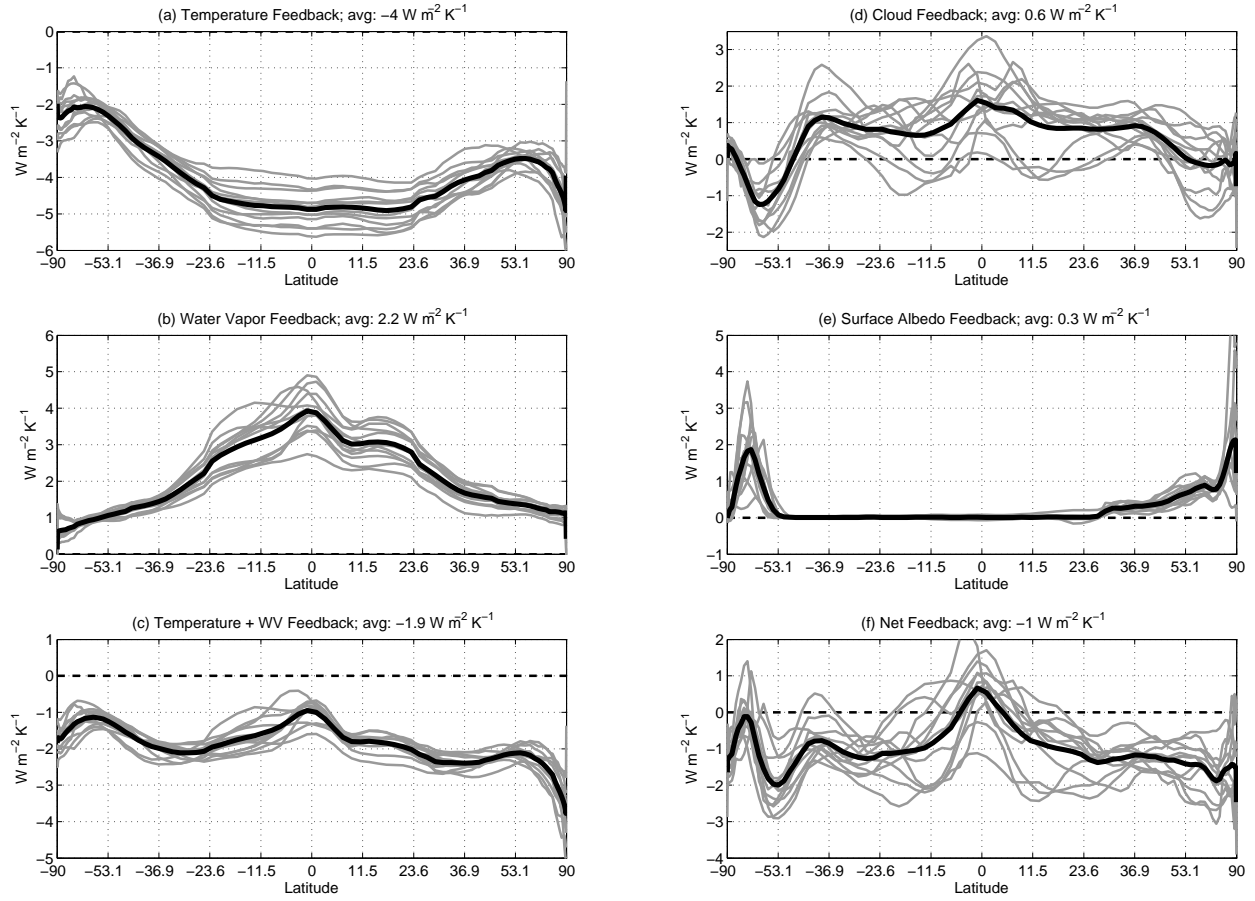


FIG. 3. Zonal mean (a) temperature, (b) water vapor, (c) combined temperature-water vapor, (d) cloud, and (e) surface albedo feedbacks, along with (f) the sum of all feedbacks. Each of the twelve models is represented by an individual gray line, and the thick black line represents the multi-model mean. The abscissa is sine of latitude so that the visual integral is proportional to Watts per Kelvin of mean surface temperature change. Note that the vertical axis limits vary among panels, but all span a range of $6 \text{ W m}^{-2} \text{ K}^{-1}$.

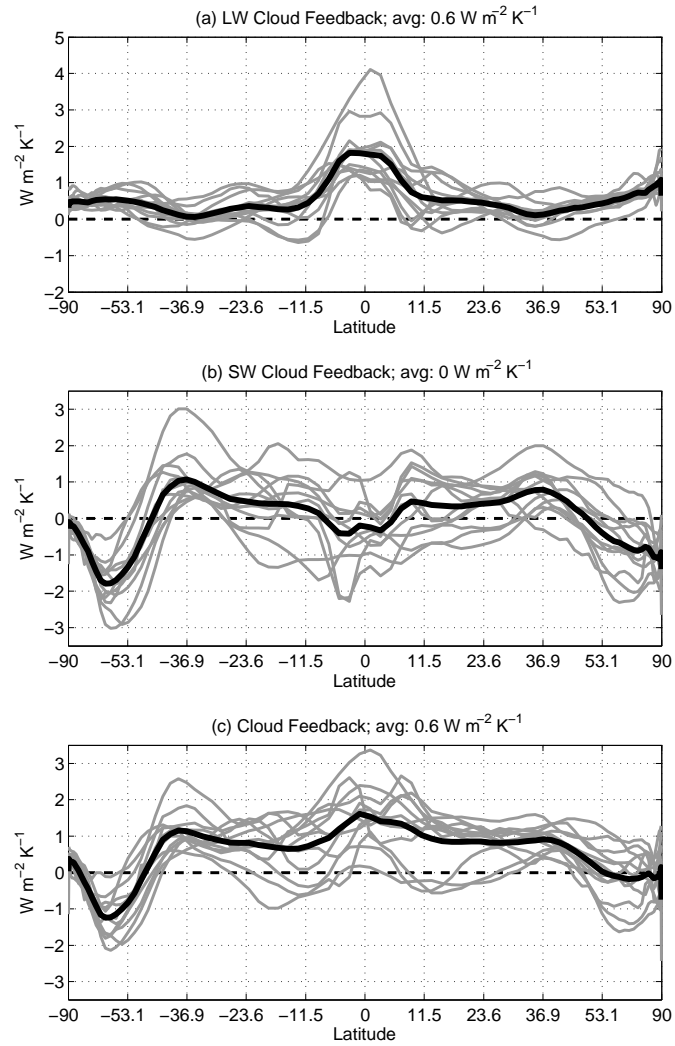


FIG. 4. As in Figure 3 but for the (a) LW, (b) SW, and (c) net cloud feedbacks. Note that the vertical axis limits vary among panels, but all span a range of $7 \text{ W m}^{-2} \text{ K}^{-1}$.

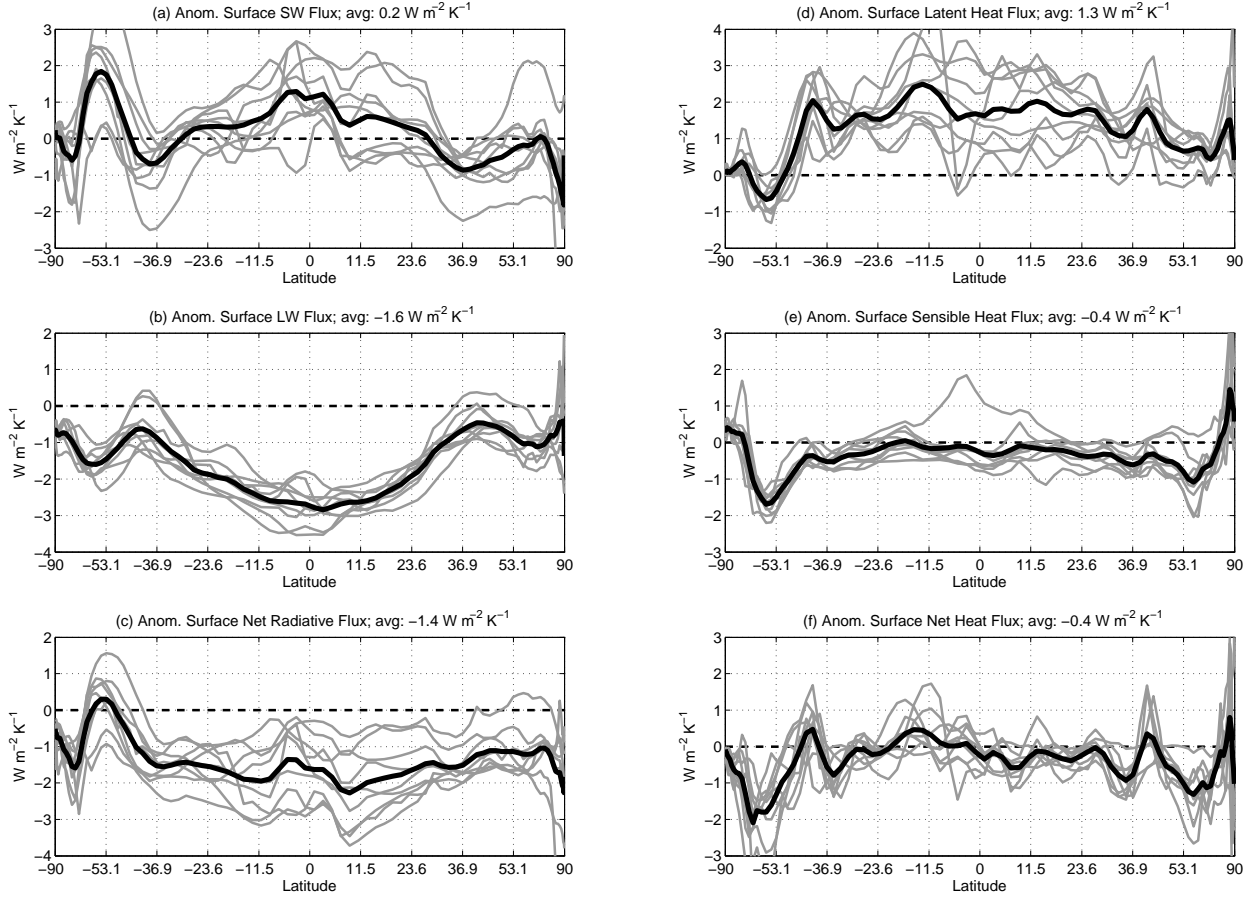


FIG. 5. Changes in surface (a) SW radiation, (b) LW radiation, (c) net radiation, (d) latent heat flux, and (e) sensible heat flux, along with (f) the sum of all terms over the 21st Century, expressed per unit of global mean temperature change. Positive anomalies represent anomalous fluxes *into* the atmosphere. Note that the vertical axis limits vary among panels, but all span a range of $6 \text{ W m}^{-2} \text{ K}^{-1}$.

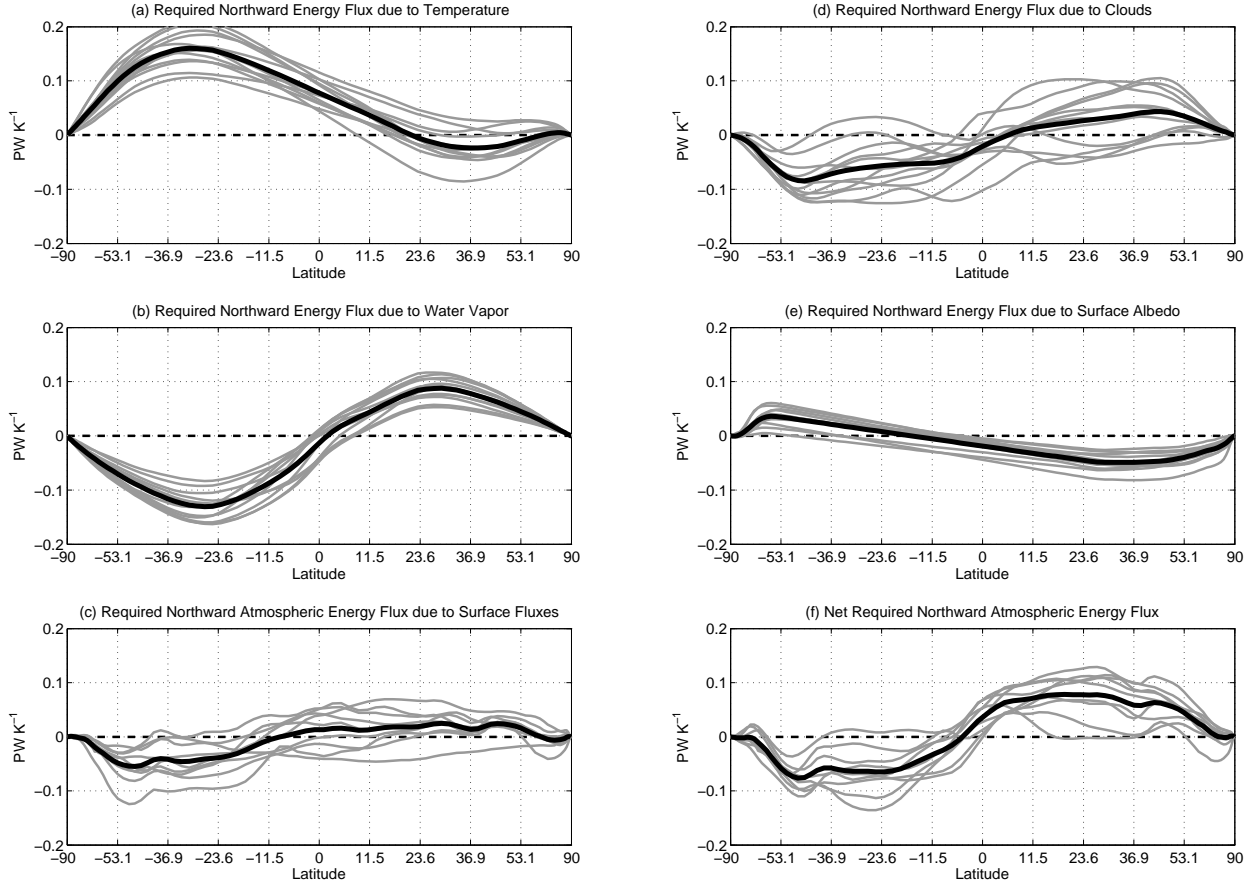


FIG. 6. Implied northward meridional heat flux anomalies in the climate system due to (a) temperature, (b) water vapor, (d) cloud, and (e) surface albedo feedbacks, and the implied *atmospheric* northward heat flux anomaly due to (c) anomalous surface fluxes and (f) the sum of TOA and surface heat flux anomalies. The implied northward energy fluxes are computed by integrating the TOA or surface flux anomalies over a polar cap as described in the text.

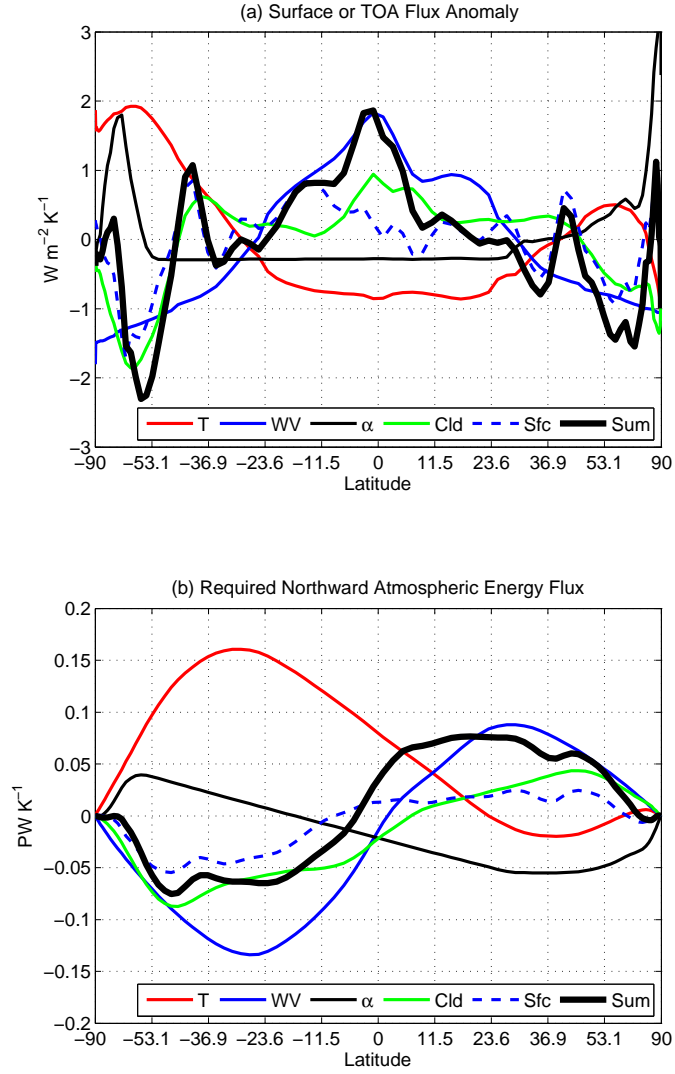


FIG. 7. (a) Multi-model mean TOA and surface flux anomalies and (b) implied northward meridional heat flux anomalies due to changes in (red) temperature, (solid blue) water vapor, (thin black) surface albedo, (green) clouds, (dashed blue) surface fluxes, and (thick black) net fluxes into the atmosphere. The TOA and surface flux anomalies are plotted as anomalies from their global means. The implied northward energy fluxes are computed by integrating the TOA net flux anomalies over a polar cap as described in the text.

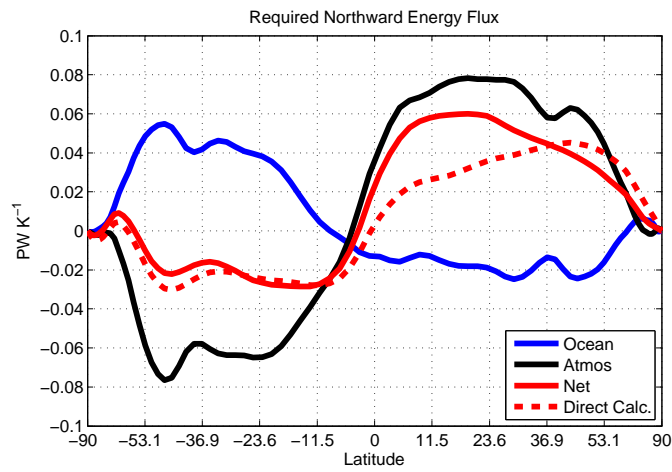


FIG. 8. The implied changes in (red solid) net poleward transport by the climate system, partitioned into components due to changes in (black) atmosphere poleward transport and (blue) the sum of oceanic transport and storage. Also provided in the red dashed line is the net transport anomaly computed directly from the ensemble mean TOA flux anomalies (i.e., without use of the radiative kernels). Note that the black curve is the same as in Figure 7.